Electron Transfer in Reaction Centers of *Blastochloris viridis*: Photosynthetic Reactions Approximating the Adiabatic Regime†

P. Huppmann,‡ S. Spörlein,‡ M. Bibikova,§ D. Oesterhelt,§ J. Wachtveitl,‡,|| and W. Zinth*,‡

Institut für BioMolekulare Optik, Sektion Physik, Ludwig-Maximilians-Universität, Oettingenstr. 67, D-80538 München, Germany, Institut für Physikalische und Theoretische Chemie, Johann-Wolfgang-Goethe-Universität, Marie-Curie-Str. 11, D-60439 Frankfurt, Germany, and Max-Planck-Institut für Biochemie, Am Klopferspitz 18a, D-82152 Martinsried, Germany

Received: December 28, 2002; In Final Form: June 17, 2003

Femtosecond time-resolved experiments on native and mutant (L168 H → F) reaction centers of *Blastchloris viridis* offer a direct approach to study the reaction mechanisms and the optimization stategies for the primary steps in the light reaction of bacterial photosynthesis. The experiments focus on a temperature-dependent analysis of reaction rates and an evaluation of the oscillatory contributions. For wild-type reaction centers the reaction times τ_{1a} (dominant component of the first electron-transfer step) and τ_2 (second electron-transfer step) decrease toward lower temperatures. τ_{1a} deceases by a factor of 1.5 between 300 and 30 K, while τ_2 decreases by a factor of 4. Interestingly, the L168 H → F mutant, which exhibits a much faster primary charge separation than wild type, shows a similar strong acceleration also for the component τ_{1a}. For both types of reaction centers, pronounced wave-packet-like absorption changes in the range of the stimulated emission are observed at low temperatures. The results are discussed within the scope of electron transfer theory. They suggest that a transition from the nonadiabatic to the adiabatic regime occurs for the fastest reactions at low temperatures and that the first reaction step must stay in the nonadiabatic regime in order to ascertain optimum photosynthetic efficiency.

I. Introduction

During the past decade time-resolved experiments with resolution in the femtosecond range led to a detailed picture of the primary reaction steps of photosynthetic electron transfer (ET) in bacterial reaction centers (RC).[1−10] The photoexcited electronic state P*, reached by optical excitation of the primary donor, the Special Pair P of bacteriochlorophyll (BChl) molecules in its long wavelength absorption band, lives for 3 ps at room temperature.[2,3,5,6,11] In the primary reaction step an electron is transferred from P* to the neighboring accessory bacteriochlorophyll B_A.[5−7,9,10,12−14] The second reaction step with electron transfer to the bacteriopheophytin (BPhe) H_A is faster. It proceeds in wild-type reaction centers at room temperature in the subpicosecond regime [0.9 ps in *Rb. sphaeroides* and 0.65 ps in *Blastochloris* (formerly called *Rhodopseudomonas*) *viridis*].[5,6,10] The primary electron-transfer ends with the slower (200 ps) reaction step to the quinone Q_A. Primary photosynthetic charge separation can therefore be described as a series of sequential electron-transfer reactions between neighboring chromophores. The energetics of the initial intermediates has been determined.[13−18] Studies show that there is a small decrease of free energy from P* to $P^+B_A^-$ and a larger one in the second step. The dynamics and energetics seem to be well-adapted for high quantum yield due to efficient and irreversible charge separation.[1,19−21] Optimization strategies within the RC were tested extensively by pigment variation and site-specific mutagenesis.

Extended experimental studies of the primary reaction have shown that the simple qualitative picture of primary electron transfer reactions presented above has to be supplemented: (i) the observation of multiphasic kinetics could be related to distributions of reaction parameters; they were partly assigned to energetic heterogeneities of the reaction center.[12,17,18,22,23] Other studies explained the multiphasic kinetics by time-dependent reorganization induced by protein motion. (ii) Upon excitation into higher lying absorption bands of the monomeric bacteriochlorin pigments of native or modified RC, alternative reaction pathways starting at the accessory bacteriochlorophyll were found.[24,25] These observations may also turn out to be important for the understanding of photosynthesis in green plants, where the spectra of the different chromophores of the photosystems overlap strongly. (iii) Experiments with high temporal resolution on bacterial reaction centers revealed oscillatory changes of the sample properties (absorption, stimulated emission, fluorescence) with frequencies in the 30−200 cm^{-1} range superimposed on the exponential ET kinetics.[26−29] Experimental studies on different preparations of reaction centers from *Rb. sphaeroides* have addressed this observation and explained it by the existence of excited-state wave packets in the Special Pair.[26,27,30] (iv) The temperature dependence of the first reaction step has been investigated for wild-type RC of *Rb. sphaeroides* and *B. viridis*.[31−33] In these publications increasing reaction rates toward low temperatures were found for the first electron-transfer reaction in RC from both species. Fleming and co-workers have seen no evidence for a B^- intermediate,[31] while Lauterwasser et al. found P^+B^- as a short-

† Part of the special issue "A. C. Albrecht Memorial Issue".

* To whom correspondence should be addressed. Tel: +49/8921809201. Fax: +49/8921809202). E-mail: zinth@physik.uni-muenchen.de.

‡ Ludwig-Maximilians-Universität.

§ Max-Planck-Institut für Biochemie.

|| Johann-Wolfgang-Goethe-Universität.

10.1021/jp027845c CCC: $25.00
Published on Web 08/06/2003

lived intermediate in *Rb. sphaeroides* and measured a strong acceleration for this second transfer step from B^- to H_A.[33]

In this paper we present new experimental results on photosynthetic electron-transfer reactions in RC of *B. viridis*. Data on the fastest ET reactions of wild-type reaction centers and the mutant L168 H → F were measured as a function of temperature, and reaction times as short as 250 fs were found. Wave packet-like oscillatory features as well as the temperature dependence of the first and the second electron-transfer reactions will be addressed. The experiments reveal that the fastest reactions are at or beyond the limits of conventional nonadiabatic electron-transfer theory.

II. Theoretical Description of Ultrafast Electron Transfer Reactions

Electron transfer from a donor D to an acceptor A can be explained in the frame of quantum mechanics by transitions between the two states DA and D^+A^-.[34] The coupling between donor and acceptor states—the electronic coupling constant V—is deduced from the overlap of the electronic wave functions of donor and acceptor. Quantum mechanics shows that for small and constant energy differences ΔE between (static) donor and acceptor states the population of the product state D^+A^- oscillates in time: $P(D^+A^-) = \sin^2(2\pi V/h)$. After a transfer time $T_{ET} = h/4V$, a complete transfer of the population has occurred for the first time. Larger values of the energy difference, $|\Delta E| \gg V$ lead to weaker population transfer. In the photosynthetic RC the donor/acceptor system is imbedded in an environment where the motions of the nuclei lead to strong fluctuations of the energy difference. The system resides for certain times at large values of $|\Delta E|$ with negligible ET. Electron transfer becomes possible only for much shorter periods, when the interaction region at $\Delta E \approx 0$ is crossed. In the most simple theoretical approach a linear dependence of ΔE with time for the rapid passing of the interaction region is assumed: $\Delta E(t) = \alpha t$. The transition probability P_{ET} for ET to the product state for each crossing of the interaction region is described by the Landau–Zener theory[34,35]

$$P_{ET} = 1 - \exp(-\gamma_{LZ}) \tag{1}$$

where

$$\gamma_{LZ} = \frac{2\pi}{\hbar}\frac{V^2}{\alpha}$$

For the standard situation of nonadiabatic ET, the Landau–Zener factor γ_{LZ} is small ($\gamma_{LZ} \ll 1$, $\gamma_{LZ} \approx P_{ET}$), and many transitions through the interaction region are required before ET is completed. Under the assumption that (i) the motion of the surroundings has a harmonic temporal dependence with the frequency ω and that (ii) the interaction region is hit twice per oscillation period, the electron-transfer becomes exponential with a reaction time $\tau_{ET} = \pi/(\omega P_{ET})$. For situations where the motion of the surroundings is not harmonic, one can replace π/ω by the typical correlation time $\tau_{\Delta E}$ of the energy difference. For simplicity, we use π/ω in the following discussion. However, the results also hold for the anharmonic case.

Another requirement for the conventional, nonadiabatic ET reaction is that the transfer is so slow that it proceeds between vibrationally equilibrated states. Here the nuclear part of the ET can be described by the thermally averaged Franck–Condon factor FC. In the most simple reaction model, only one vibrational mode of constant frequency ω is used to describe the nuclear motion and the Franck–Condon factor can be expressed as a function of ω, the temperature T, the difference in free energy between initial and final state ΔG, and the reorganization energy λ.[36–38]

$$k_{ET}(T) = \frac{1}{\tau_{ET}} = \frac{2\pi}{\hbar}V^2\mathrm{FC} \tag{2}$$

where

$$\mathrm{FC} = \frac{1}{\hbar\omega}e^{-S(2\upsilon+1)}I_P(2S\sqrt{\upsilon(\upsilon+1)})\left(\frac{\upsilon+1}{\upsilon}\right)^{P/2} \tag{3}$$

where

$$S = \frac{\lambda}{\hbar\omega} \quad P = \frac{\Delta G}{\hbar\omega} \quad \upsilon = 1/(e^{\hbar\omega/kT} - 1)$$

I_P is the modified Bessel function. For $kT \gg \hbar\omega$, FC can be approximated by the high-temperature value FC_{HT}:

$$\mathrm{FC}_{HT} = \frac{1}{\sqrt{2\pi\lambda kT}}\exp(-E_A/kT) \tag{4}$$

with the activation energy $E_A = (\Delta G - \lambda)^2/4\lambda$.

Considering the conventional description and the nonactivated case, one can relate the Landau–Zener factor γ_{LZ} with the parameters of eqs 2–4:

$$\gamma_{LZ} = \frac{\pi}{\omega\tau_{ET}} \tag{5a}$$

$$\gamma_{LZ} = \frac{\pi}{\omega\tau_{ET}} \approx \frac{2\pi^2V^2}{\hbar\omega\sqrt{2\pi\lambda kT}} \qquad kT \gg \hbar\omega \tag{5b}$$

While eq 5a is valid without restriction for the nonadiabatic electron transfer, eq 5b can only be used for high temperatures $kT \gg \hbar\omega$. In the case of standard nonadiabatic reactions, γ_{LZ} is small and the transfer time is always much larger than the nuclear vibrational period $2\pi/\omega$ and the pure electronic transfer time T_{ET}. Adiabatic features become important when the Landau–Zener factor approaches unity. Here a high probability $P_{ET} \approx 1$ for the transition to the product state occurs at each crossing of the interaction region. In this "adiabatic" situation the time dependences of the populations no longer remain exponential and the reaction speed is controlled essentially by the time required to reach the interaction region, i.e., ET is controlled by the nuclear motion. If the preparation of the initial state (for the experiments on the photosynthetic RC this is the optical excitation P → P*) is independent of the actual value of ΔE, one can estimate that the ET occurs on the time scale of the vibrational period within $\tau_{ET} \approx \pi/\omega$. When the oscillatory motion is in phase with the preparation, stepwise or oscillatory features may be observed in the ET process. When the preparation leads directly to the interaction region the initial transfer is determined by the undisturbed reaction time T_{ET} given above.

The application of standard ET theory for the initial ET reaction at room temperature can be well-justified from the consistency of assumptions and model parameters: Modeling of the primary electron transfer from P* to B_A in native reaction centers (which proceeds in ≈2 ps) yields a set of values: $V \cong 20\ \mathrm{cm}^{-1}$, $\hbar\omega = h\nu \approx 100\ \mathrm{cm}^{-1}$, $\Delta G \approx 400–600\ \mathrm{cm}^{-1}$, $\lambda \cong 400–600\ \mathrm{cm}^{-1}$. Indeed, the observed reaction time of 2 ps is much longer than the vibrational period (330 fs). Thus γ_{LZ} becomes small ($\gamma_{LZ} = 0.05$) and the area of validity of standard nonadiabatic electron transfer theory is not left. In addition, the

reaction time is longer than a typical vibrational relaxation time of $T_1 \approx 0.5$ ps which can be estimated from the IR line widths of the P* state observed in transient IR experiments.

However, when addressing the subpicosecond ET reactions presented below, e.g. the second and faster electron-transfer step in the wild-type RC and the accelerated primary reaction step of some mutants or reactions at low temperatures, the parameter range of nonadiabatic conventional electron-transfer theory may be left.

III. Experimental Section

The measurements of the primary reaction dynamics are performed by the excite and probe technique using a femtosecond laser system. The basic features of the experimental setup have been described in detail elsewhere.[21,30] Special features important for the experiments presented here are the femtosecond laser system consisting of a Ti:sapphire laser operated at a central wavelength of 870 nm and a regenerative amplifier (repetition rate 20 Hz, output pulse duration 100 fs). The amplified pulses were split into two parts. One part (40 μJ) is frequency-doubled and converted by a noncollinear optical parametric amplifier to $\lambda = 970$ nm (0.3 μJ) at a pulse duration of 40 fs.[39] This pulse is used to excite the sample in the Q_y P-band (diameter of excitation spot at the sample $\approx$ 0.3 mm). Another part (1−2 μJ) from the amplifier output was focused into a 2 mm sapphire crystal to generate a white light continuum. After recompression and spectral filtering ($\Delta\lambda \approx 20$ nm) in a grating setup this part was used for probing. The time resolution of the experiment is related to the width of the cross correlation function between the excitation pulse at 970 nm and the tuneable probe pulse. For probing between 1020 and 1100 nm the width of the cross correlation function was determined to be around 90 fs. Pump and probe pulses (parallel polarization) were crossed in the sample cell at a small angle of 3°. The probing light pulses had an energy well below 10 nJ. For every time delay between exciting and probing pulses, the change in transmission of the probing pulse was averaged over 1000 single shots. The data points presented in Figures 2 and 4−6 were obtained by averaging over repetitive scans (≈10 times). In Figures 2 and 5, the data are plotted on a linear time scale until $t_D = 1$ ps; for later delay times, a logarithmic scale is used.

The calculated curves presented in Figures 2 and 4−6 are model functions consisting of a sum of exponentials convoluted with the instrumental response function. This procedure models reactions where pairs of intermediate states *i* and *j* are connected via microscopic reaction rates γ_{ji} and γ_{ij}. The use of reaction rates is justified within the scope of nonadiabatic electron-transfer theory.

Wild type (WT) reaction centers of *B. viridis* and of the mutant L168 H → F were prepared according to the procedure given in refs 40 and 41. Since the experiments also had to be performed at cryogenic temperatures, where a continuous exchange of the irradiated volume between two laser shots is not possible, the accumulation of long-lived photoproducts could be avoided by adding 0.32 mM benzyl viologen to the sample. This presumably caused a prereduction of the quinones. The effect of benzyl viologen was controlled in test experiments, where we found only weak changes of the femtosecond dynamics of the treated reaction centers at repetition rates up to 50 Hz. To obtain clear samples at cryogenic temperatures, the reaction center preparations contained 52% (v/v) glycerol as cryoprotector. The minor differences between the time constants found here at room temperature and the corresponding literature values[41] are due to the sample treatment by benzyl viologen and the presence of glycerol. The concentration of the reaction center preparation was adjusted to yield a transmission at room temperature at 960 nm between 10% and 20%.

In the L168 H → F reaction center histidine L168 was replaced by a phenylalanine as described previously.[40−42] This point mutation changes important properties of the reaction centers: (i) The hydrogen bond between L168 and the acetyl group of the BChl molecule P_L is removed. (ii) X-ray structure analysis shows a rotation of the ring I acetyl group of P_L and a related approach to P_M. [43] (iii) The Q_Y absorption peak of the Special Pair P band is shifted to shorter wavelengths, and at low temperatures it becomes evident that the Special Pair band consists of two components (see Figure 1). (iv) In contrast to wild-type reaction centers, the position of the P absorption band of the mutant does not change considerably upon cooling (see Figure 1b). (v) The mutation changes the exciton coupling between the bacteriochlorophylls, as can be seen from the pronounced differences between the absorption spectra of wild-type reaction centers and mutated reaction centers in the Q_Y-range of the BChl around 830 nm. (vi) The primary electron transfer reaction at room temperature is strongly accelerated. This is believed to be due to the changed energetics of the Special Pair and/or modifications of the electronic coupling between P and B_A.[44] The latter could be caused by differences in charge distribution within P or in an altered geometric arrangement induced by the mutation.

IV. Results

Wild-Type Reaction Centers. The first set of time-resolved data is taken in the spectral range from 1020 to 1100 nm, i.e., in a spectral region where the signal is dominated by stimulated emission from the excited Special Pair P*. The temperature dependence of the signal is shown for WT RC in Figure 2, left panel, for a probing wavelength of 1040 nm. At room-temperature one observes a negative absorbance change due to stimulated emission. Its recovery can be fitted by a biexponential model function with the two time constants of $\tau_{1a} = 2.2$ ps and $\tau_{1b} = 12$ ps with a relative amplitude ratio of 1.9. At lower temperatures the decay of stimulated emission (and with that the decay of the excited electronic state P* via electron transfer to $P^+B_A^-$) is accelerated. At 70 and 30 K one finds the fast component (relative amplitude of 75%) with decay times of $\tau_{1a} = 1.2$ and 1.1 ps, respectively. Throughout the whole temperature range the slower component remains longer than $\tau_{1b} = 10$ ps. The temperature dependence of the fast time constant is summarized in Figure 3 (open circles).

Oscillatory features are visible when the data are plotted on an enlarged scale (see Figure 4). In the long wavelength part of the stimulated emission (1060 and 1100 nm), pronounced modulations are visible that decay on the time scale of 1 ps. Toward shorter wavelengths the modulations of the signal become weaker. They vanish at 1020 nm, a wavelength that is close to the peak of the stimulated emission. At low temperature (70 K; Figure 4, right) similar oscillations are visible. The thin lines in Figure 4 represent the residual absorbance changes obtained by subtracting the experimental data from the exponential model curve. They clearly display details of the oscillatory behavior. It should be noted that the phase of the oscillation (at low temperatures) is constant for $\lambda > 1040$ nm. However the oscillation phase is shifted by π at 1020 nm. A Fourier transform of the residual absorbance changes has been performed in order to determine the oscillation frequencies. An example is given for $\lambda_{pr} = 1060$ nm in Figure 4 (bottom). The analysis yields the main contribution to the oscillatory features

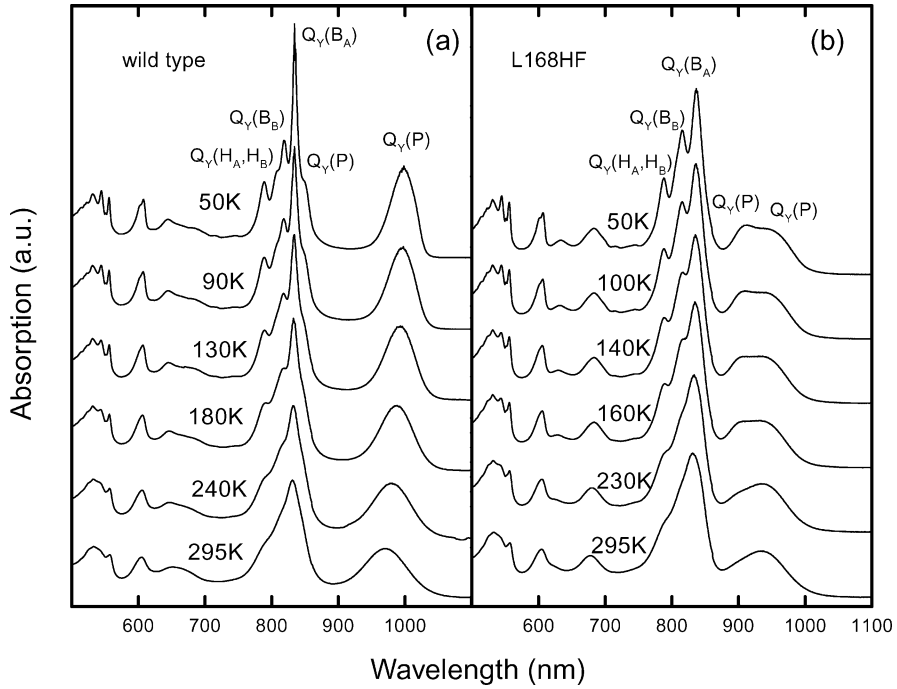

Figure 1. Temperature-dependent optical absorption spectra of wild type (left) and L168 H → F mutant RC (right) from *B. viridis* in Tris/LDAO buffer (pH7) and 52% (v/v) glycerol. Note especially the different location and temperature-dependent response of the upper and lower exciton signal of the Q_Y(P) band between 800 and 1000 nm.

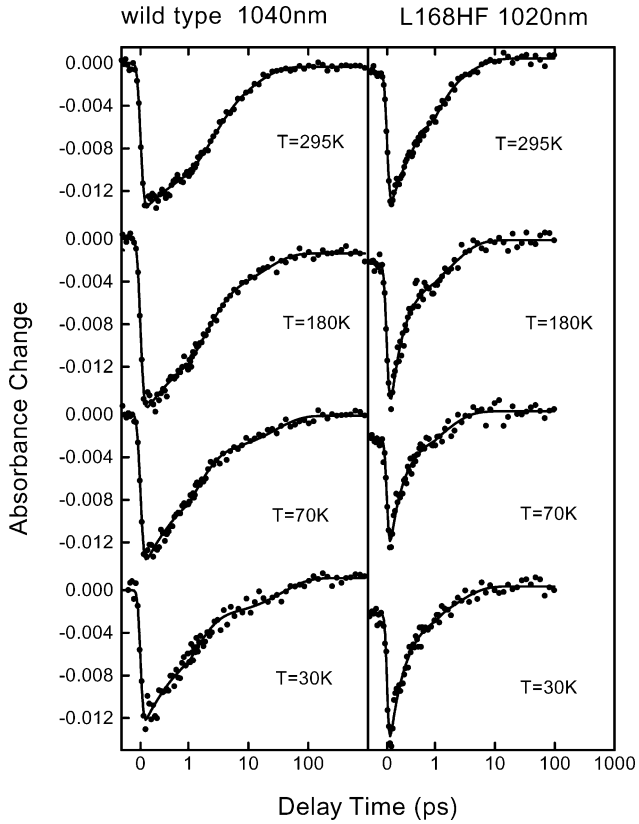

Figure 2. Temperature-dependent transient absorbance changes of wild type (left) and L168 H → F mutant RC (right) for a respective probe wavelength, close to the maximum of the stimulated emission signal. Solid points represent the experimental data; model functions of the data using the time constants given in the text are displayed as solid lines. The acceleration and biphasic character becomes more pronounced toward low temperatures.

at a frequency of 150 cm^{-1}. Weaker components appear around 70 cm^{-1} (room temperature) and ≈30 cm^{-1} (70 K).

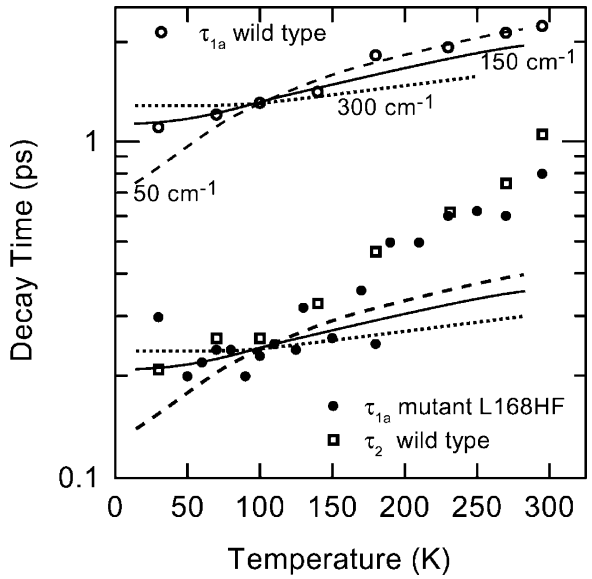

Figure 3. Time constants for the first (WT, open circles, L168 H → F, filled circles) and second (WT, open squares) electron-transfer step as a function of temperature. Curves: Modeling of the ET using standard theory for the activation-less case for three values of the vibrational frequency: $\hbar\omega = 300$ cm^{-1} (dotted), 150 cm^{-1} (solid), and 50 cm^{-1} (dashed).

The secondary electron transfer from B_A^- to H_A can be detected for reaction centers of *B. viridis* in a clear way at probing wavelengths of 820 nm, i.e., in a range with strong B_A absorption.[10] The exact probing wavelength was selected in a way to have minimal amplitudes from the τ_{1a} component.The initial signal rise is due to the excited-state absorption of P*. The subsequent kinetics are related to the electron-transfer reactions. Since the time constants for the first electron-transfer step are well-determined by the experiments taken in the stimulated emission region (see Figure 2), the strong fast component observed in Figure 5 ($\lambda_{pr} = 820$ nm) is directly related to the secondary electron-transfer step: From Figure 5

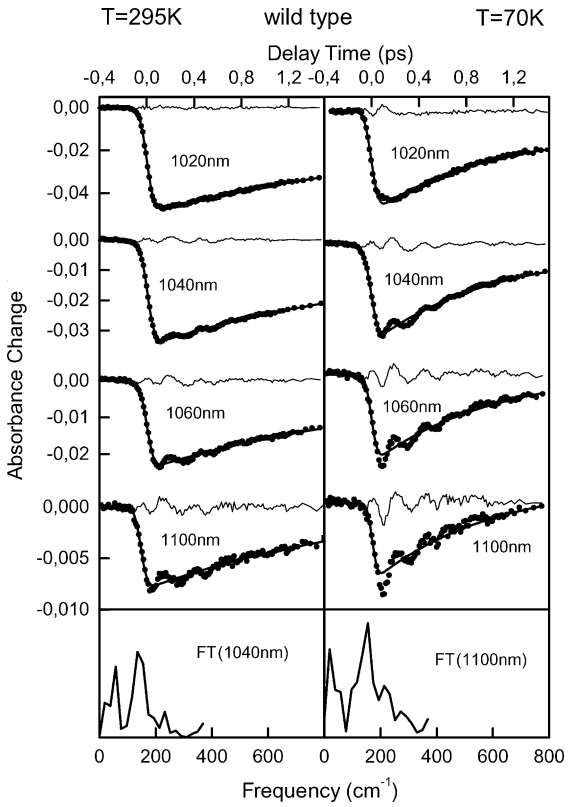

Figure 4. Top: transient absorbance changes and corresponding residuals for selected probing wavelengths of wild-type RC for room temperature (left) and 70 K (right). Toward the long wavelength side of the stimulated emission signal, oscillatory components become more pronounced. Bottom: In both cases, the frequency of the dominant mode is around 150 cm^{-1}, as can be seen from the Fourier spectrum of the residual.

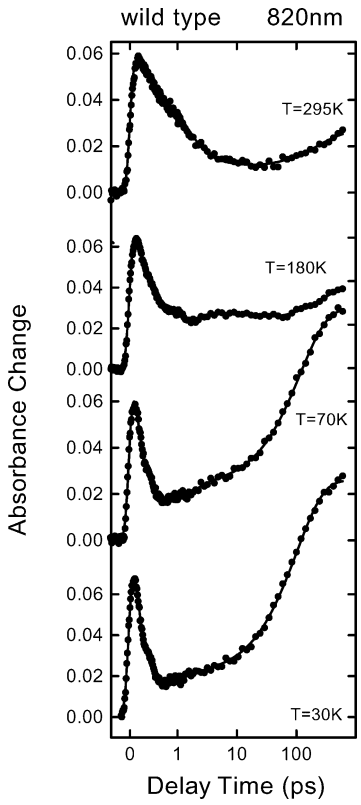

Figure 5. Kinetics of transient absorbance signals of WT RC recorded for different temperatures in a spectral region (λ_{pr} = 820 nm) dominated by contributions from the secondary ET step from B_A to H_A.

one obtains time constants between τ_2 = 1000 fs (295 K) and τ_2 = 250 fs (30 K). The temperature dependence of τ_2 determined from the complete set of experiments is plotted in Figure 3 (open squares). The strong absorbance increase on the 100 ps time domain is related to the electron transfer to the quinone Q_A. Another interesting feature appears at low temperatures during the initial signal decay: This decay is modulated with a shoulder around 300 fs. Taking the distance between initial absorption peak and this shoulder as an estimate for a highly damped oscillatory motion, we can again assign a frequency of 150 cm^{-1} to this motion.

Results for L168 H → F Reaction Centers. The temperature dependence of the primary reaction in the L168 H → F reaction centers measured at 1020 nm is shown in Figure 2 (right side). At room temperature the decrease of stimulated emission is considerably faster for the mutated reaction center than for the wild type. A biexponential fit (solid curve) yields time constants of τ_{1a} = 720 fs and τ_{1b} = 3.5 ps. The same time dependence was obtained in an earlier series of experiments, where a monoexponential fit with τ_1 = 1.1 ps was used to simulate the experimental data.[41] Toward lower temperatures a strong acceleration of the fast time constant τ_{1a} can be observed. At 150 K a value of 250 fs is reached. Only weak acceleration of the initial electron transfer occurs below 150 K. Within the whole temperature range from 300 to 30 K the slower component does not change significantly. The temperature dependence of the reaction time τ_{1a} of the mutant L168 H → F obtained from a series of experiments on three independently prepared reaction center samples is plotted in Figure 3 (filled circles).

Experiments around 820 nm probing wavelength (data not shown) reveal pronounced features due to the secondary electron transfer from B_A^- to H_A. There is also a speeding up of the secondary reaction rate toward lower temperatures. The values are similar to those found in wild-type reaction centers. However, since the two time constants τ_{1a} and τ_2 become very similar at low temperatures, an accurate determination of τ_2 is not possible at 820 nm and we will not use these results in the further discussion.

Oscillatory changes of the absorption transients for the L168 H → F reaction centers can be seen in Figure 6, where the early absorption changes are plotted on a linear scale. At room temperature the mutated reaction centers do not display distinct oscillatory absorption changes. At low temperatures (see Figure 6, right) the oscillations appear as steps in the very fast decay of the stimulated emission. These steps are also well-displayed in the residual absorption changes, where the subtraction of the fit of the exponential kinetics yields sinusoidal oscillations in the residual. In the mutated RC the amplitudes of the oscillations scale linearly with the amplitude of the fast component of the stimulated emission. Even at 1020 nm, there is no deviation from this behavior and there is no change of the phase of the modulation. Fourier analysis of the residual absorption changes shows that the dominant oscillation occurs at the same frequency of 150 cm^{-1} as in wild-type RC. A weaker component at a frequency of 70 cm^{-1} also contributes to the signal.

The experimental observations can be summarized as follows: For wild-type reaction centers of *B. viridis*, we observed a decrease of the reaction time τ_{1a} and τ_2 to lower temperatures. τ_{1a} decreases by a factor of 1.5 between 300 and 30 K, while τ_2 decreases by a factor of 4. A similar decrease occurs in the component τ_{1a} of the mutated RC L168 H → F. For wild-type RC we find pronounced wave-packet-like absorption changes in the range of the stimulated emission at room temperature as

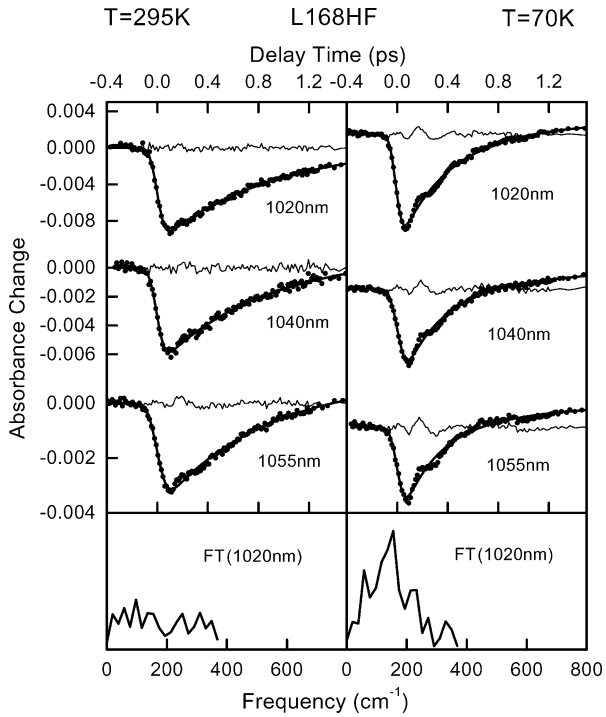

Figure 6. Top: transient absorbance changes and corresponding residuals for selected probing wavelengths of RC of the mutant L168 H → F for room temperature (left) and 70 K (right). At low temperatures, oscillatory components are visible. Bottom: the Fourier spectrum of the residual taken at 1020 nm. Only at low temperatures a pronounced peak appears around 150 cm^{-1}.

well as at low temperatures. Mutated reaction centers L168 H → F show wave-packet-like features only at low temperatures.

V. Discussion

In the following we focus on the observation of extremly fast reaction times at low temperatures and on the oscillatory absorption changes in the context of a potential adiabaticity of the ET reactions. For the primary reactions we treat the dominant and most rapidly reacting part represented by the time constant τ_{1a}. The unexpected strong acceleration of the ET toward low temperatures will be discussed in a forthcoming paper. In this discussion we treat the electron-transfer reaction coupled to a single vibrational mode. Coupling to multiple modes could lead to differing results. However, the conclusions given below should remain valid at least in a qualitative way.

What Is the Relevant Vibrational Frequency? According to the definition of the Landau−Zener parameter γ_{LZ} and eq 5, knowledge of the vibrational frequency ω is required to assign a reaction to the adiabatic or the nonadiabatic regime. Different techniques have been used to determine the vibrational frequency: Molecular dynamics simulations have shown that the autocorrelation function of ΔE decays on the time scale of 100 fs.[45,46] From this observation we conclude that the frequency should be in the range $\hbar\omega \approx 300$ cm^{-1} [45,46] Conventional approaches describe the influence of a polar environment via the longitudinal relaxation time τ_{long}. For a typical polar solvent like DMSO τ_{long} can be estimated to be on the order of 1 ps or $\hbar\omega = h/\tau_{long} \approx 30$ cm^{-1}. More direct experimental methods can be used to determine hω from the temperature dependence of the ET time. Equations 2 and 3 show that at temperatures $kT > \hbar\omega$ (where the reaction is in the high-temperature limit) one finds the Arrhenius-type slowing down for a thermally activated reaction, while an acceleration with $1/(T)^{1/2}$ occurs for the activation-less case. Both temperature dependencies level off around $kT \approx \hbar\omega/2$. This is illustrated by the various curves in Figure 3, where the reaction times are plotted for activation-less ET for vibrational frequencies of 50, 150, and 300 cm^{-1}. Comparing these curves with the experimental traces yields information on the relevant mode: The similarities of the different experimental traces with the weak changes of the reaction times below 100 K indicate that $\hbar\omega$ is 70−200 cm^{-1}. The increase in reaction time for some ET reactions at higher temperatures is out of the range of the conventional description and can be explained, for example, by a temperature dependence of the electronic coupling V.[44,47,48] However, this assumption alone cannot explain the different observations such as the temperature dependence of WT τ_{1a} (with a weak acceleration between 300 and 100 K), WT τ_2 (with a strong acceleration), τ_{1a} of L168 H → F (strong acceleration) or the strong deceleration of the reaction with decreasing temperature in the M208FL mutant.[44]

As a consequence, we use $\hbar\omega = 100$ cm^{-1} as a typical vibrational frequency for the following discussion.

Are Oscillatory Absorption Transients an Indication for Adiabatic Electron Transfer? In various experiments on RC from different photosynthetic bacteria, pronounced modulations of the absorption changes could be observed. Here we focused on RC from *B. viridis*, where strong modulations are seen in the wavelength range with large signal from stimulated emission. The Fourier transformation yielded peaks of the spectra around 70 and 150 cm^{-1}. For the wild-type RC, where the most pronounced modulations are seen, the oscillations are strongest in the long wavelength range of the stimulated emission band. They are weak and have opposite sign at 1020 nm, close to the peak of the stimulated emission band. These observations are similar to those obtained by Vos et al. [27] for the RC of *Rb. sphaeroides*, where this wavelength dependence led to the conclusion that the modulations are related to the motion of a vibrational wave packet in the excited electronic S_1 state, modulating directly the stimulated emission. As a consequence, these features cannot be taken as an indication for a modulated electron-transfer reaction in the adiabatic regime. This conclusion is supported by the theoretical discussion given above, indicating that for $\tau_{1a} \approx 1.1$ ps (30 K) and $T_{vib}/2 = \pi/\omega \approx 1/(2 \times 100$ $cm^{-1}) \approx 170$ fs, the Landau−Zener factor according to eq 5a becomes 0.17 and thus the reaction should be essentially nonadiabatic. Consequently, no modulation of the ET by vibrational motion should be visible. The situation changes for the mutated RC L168 H → F. Here the reaction time is ≈250 fs at low temperatures and adiabatic features should be more evident. For L168 H → F we find modulations of the rapidly decaying signal throughout the entire investigated gain region, even at 1020 nm. The Fourier transformation of the residual absorption changes leads to a very similar spectrum as for the wild type RC. The time dependence of the signal behaves as expected for a modulated ET, where the transition to the product, i.e., the interaction region, is reached after half the oscillation period after optical excitation (170 fs). However, even if these oscillations behave as expected for a modulated ET (stepwise signal decay, nonvanishing modulations at the peak wavelength of the stimulated emission), we cannot definitely rule out that a modulation of the stimulated emission causes the observed modulations. To decide this question, further and more extensive experiments performed over a wider range of probing wavelengths are required.

Electron Transfer in RC of *B. viridis* at *R*oom Temperature Is Nonadiabatic. At room temperature the fastest ET

times of the wild-type RC are around 1 ps ($\tau_{1a} \approx 2.2$ ps, $\tau_2 \approx 1.0$ ps). When an average value of the vibrational frequency of $\hbar\omega = 100$ cm^{-1} is used, the Landau−Zener factor obtained from eq 5 is 0.07 and 0.17, respectively. As a consequence, even the fastest room-temperature reaction is well in the nonadiabatic regime. The theoretical modeling of the initial ET reaction by nonadiabatic theory is well-justified at room temperature.

Electron-Transfer Reactions at Low Temperatures beyond the Limits of Nonadiabtic Theory. The strong acceleration of some ET reactions at low temperatures leads to large values of the Landau−Zener factor: If we use the relation of eq 5a we obtain Landau−Zener factors of $\gamma_{LZ} = 0.67$ for the secondary ET of the wild-type RC and for the primary ET of the mutant L168 H → F. In other words, the ET reaction, modeled by an exponential time dependence, has a time constant (250 fs) that is very close to the time of the relevant nuclear motion (170 fs). According to the conventional concepts of the ET reaction described above, the reaction proceeds here with the ultimate speed allowed for an ET process in the specific surrounding. The reaction becomes medium-controlled.

Adiabatic Reactions and the Optimization of Photosynthetic ET. The photosynthetic RC is an energy conversion system optimized for highest quantum yield (0.97)[49] of the charge-separation process and optimal use of the photon energy. This is accomplished by the stepwise reaction scheme, where each intermediate has fast forward reaction speed and minimum recombination yield.[1,20] Theoretical arguments indicate that the ratio of forward to recombination rate should be large for each reaction step. For the set of sequentially populated intermediates, the yield of the final intermediate is of importance. Considering the reaction steps in the RC, it becomes evident that the recombination from a certain intermediate depends on the ET parameters (e.g. the electronic coupling V) of the preceding reaction step. This can be demonstrated for the first radical pair state P^+B^-. This intermediate is most efficiently formed if the initial ET from P* to B (rate γ_1) is as fast as possible, to compete with the recombination from P* to the ground-state P by internal conversion (rate γ_{IC}). The quantum efficiency for the formation of P^+B^- becomes

$$\eta(P^+B^-) = \gamma_1/(\gamma_1 + \gamma_{IC}) \tag{6}$$

For efficient photosynthesis the quantum efficiency for the formation of the later photoproducts is mandatory. For the secondary intermediate, the radical pair state P^+H^-, η can be estimated to be

$$\eta(P^+H^-) = \gamma_1/(\gamma_1 + \gamma_{IC})\gamma_2/(\gamma_2 + \gamma_{recomb}) \tag{7}$$

where $\gamma_2 \approx 1/\tau_2$ is the rate of formation of P^+H^-, and γ_{recomb} is the recombination rate of P^+B^- to the ground state P. When all these reactions are in the nonadiabatic regime, both γ_{recomb} and γ_1 depend quadratically on their electronic coupling elements V_{PB} and V_{P*B}. For an optimized system recombination is slow and the forward reaction is fast. Here eq 7 can be approximated by

$$\eta(P^+H^-) \approx 1 - \gamma_{IC}/\gamma_1 - \gamma_{recomb}/\gamma_2 \tag{8}$$

Within the nonadiabatic limit this becomes

$$\eta(P^+H^-) \approx 1 - a/V_{P*B}{}^2 - V_{PB}{}^2/b \tag{9}$$

where a and b are constants, independent of V_{P*B} and V_{PB}. The forward and the recombination reaction occur between the same two molecules: the forward reaction from the excited-state P* to the accessory BChl B (with V_{P*B}) and the recombination from the reduced B^- to P^+ (with V_{PB}). Therefore, it is reasonable to assume that the related electronic coupling elements are proportional to each other: $V_{PB} = \kappa V_{P*B}$. When the electronic coupling V_{PB} between P and B is increased, the second and the third term in eq 8 and 9 are changed. The situation is visualized in Figure 7, where the nonadiabatic (solid) and the adiabatic case (dashed) are compared for reasonable values of the loss parameters and equal electronic coupling elements, $\kappa = 1$ (in the more general case, $\kappa \neq 1$, most of the conclusions drawn below are also valid): For small coupling the efficiency $\eta(P^+H^-)$ is small, since the internal conversion of P* dominates. A growth in V_{PB} increases both the forward reaction rate γ_1 and the recombination rate γ_{recomb}. Initially $\eta(P^+H^-)$ also rises, since the influence of the internal conversion (second term) is reduced. At large V_{PB} values, however, the third term becomes dominant and $\eta(P^+H^-)$ is lowered by increased recombination (third term). When the initial ET step approaches the adiabatic regime, γ_1 ceases to grow while the increase in recombination rate—not yet in the adiabatic regime—continues $\propto V_{PB}{}^2$. This dependence leads to a reduction in quantum yield $\eta(P^+H^-)$. In other words: for optimum quantum efficiency, the first ET step must reach highest speed to compete with internal conversion while the electronic coupling is kept as low as possible. Otherwise, the recombination from P^+B^-, which depends on the same coupling element reduces the overall efficiency. The situation in the native reaction centers seems to consider this behavior: here at room temperature, the values of γ_{LZ} show that the early forward reactions are very fast but are still in the nonadiabatic regime, preventing the described loss caused by recombination.

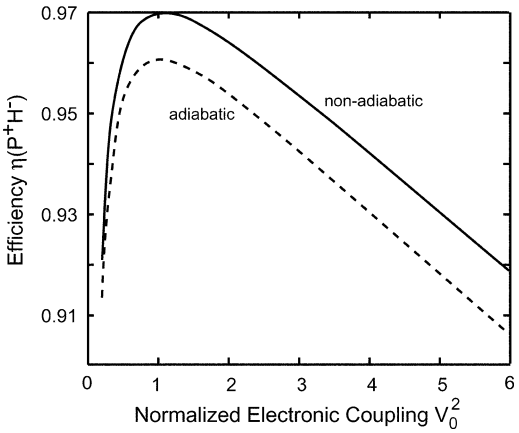

Figure 7. Quantum efficiency for the formation of the radical pair $P^+H_A^-$ according to eq 7 for the nonadiabatic (solid, $\gamma_1 = 1/(2\text{ ps}) \times V_0{}^2$) and the adiabatic case plotted as a function of normalized electronic coupling V_0. A Landau−Zener factor of 2 is assumed for a normalized electronic coupling $V_0{}^2 = 1$ for the adiabatic situation. Other constants: $\gamma_2 = 1/(1\text{ ps})$, $\gamma_{recomb} = 1/(70\text{ ps}) \times V_0{}^2$, $\gamma_{IC} = 1/(120\text{ ps})$.

In conclusion, the investigations presented here have shown that the primary reactions in the photosynthetic reaction centers at room temperature can be described in the framework of standard nonadiabatic electron transfer theory. At low temperatures extremely fast electron-transfer reaction times in the range of 250 fs have been observed, pushing these reactions beyond the limits of nonadiabatic theory.

Acknowledgment. The studies were supported by the Deutsche Forschungsgemeinschaft (SFB 377, TP B4).

References and Notes

(1) Zinth, W.; Huppmann, P.; Arlt, T.; Wachtveitl, J. *Philos. Trans. R. Soc. London A* **1998**, *356*, 465−476.

(2) Martin, J.-L.; Breton, J.; Hoff, A. J.; Migus, A.; Antonetti, A. *Proc. Natl. Acad. Sci. U.S.A.* **1986**, *83*, 957−961.

(3) Breton, J.; Martin, J.-L.; Migus, A.; Antonetti, A.; Orszag, A. *Proc. Natl. Acad. Sci. U.S.A.* **1986**, *83*, 5121−5225.

(4) Kirmaier, C.; Holten, D. *Proc. Natl. Acad. Sci. U.S.A.* **1990**, *87*, 3552−3556.

(5) Holzapfel, W.; Finkele, U.; Kaiser, W.; Oesterhelt, D.; Scheer, H.; Stilz, H. U.; Zinth, W. *Chem. Phys. Lett.* **1989**, *160*, 1−7.

(6) Holzapfel, W.; Finkele, U.; Kaiser, W.; Oesterhelt, D.; Scheer, H.; Stilz, U.; Zinth, W. *Proc. Natl. Acad. Sci. U.S.A.* **1990**, *87*, 5168−5172.

(7) Arlt, T.; Schmidt, S.; Kaiser, W.; Lauterwasser, C.; Meyer, M.; Scheer, H.; Zinth, W. *Proc. Natl. Acad. Sci. U.S.A.* **1993**, *90*, 11757−11761.

(8) Chan, C. K.; Di Magno, T. J.; Chen, L. X. Q.; Norris, J. R.; Fleming, G. R. *Proc. Natl. Acad. Sci. U.S.A.* **1991**, *88*, 11202−11206.

(9) Beekman, L. M. P.; Jones, M. R.; van Stokkum, I. H. M.; van Grondelle, R. In *Photosynthesis: from Light to Biosphere*; Mathis, P., Ed.; Kluwer Academic Publishers: Norwell, MA, 1995; Vol. I; pp 495−498.

(10) Dressler, K.; Umlauf, E.; Schmidt, S.; Hamm, P.; Zinth, W.; Buchanan, S.; Michel, H. *Chem. Phys. Lett.* **1991**, *183*.

(11) Woodbury, N. W.; Becker, M.; Middendorf., D.; Parson, W. W. *Biochemistry* **1985**, *24*, 7516−7521.

(12) Hamm, P.; Gray, K. A.; Oesterhelt, D.; Feick, R.; Scheer, H.; Zinth, W. *Biochim. Biophys. Acta* **1993**, *1142*, 99−105.

(13) Schmidt, S.; Arlt, T.; Hamm, P.; Huber, H.; Nägele, T.; Wachtveitl, J.; Meyer, M.; Scheer, H.; Zinth, W. *Chem. Phys. Lett.* **1994**, *223*, 116−120.

(14) Schmidt, S.; Arlt, T.; Hamm, P.; Huber, H.; Nägele, T.; Wachtveitl, J.; Zinth, W.; Meyer, M.; Scheer, H. *Spectrochim. Acta* **1995**, *A 51*, 1565−1578.

(15) Woodbury, N. W.; Parson, W. W.; Gunner, M. R.; Prince, R. C.; Dutton, P. L. *Biochim. Biophys. Acta* **1985**, *851*, 6−22.

(16) Parson, W. W.; Chu, Z.; Warshel, A. *Biochim. Biophys. Acta* **1990**, *1017*, 251−272.

(17) Ogrodnik, A.; Volk, M.; Michel-Beyerle, M. E. In *The Photosynthetic Bacterial Reaction Center: Structure and Dynamics*; Breton, J., Verméglio, A., Eds.; Plenum Press: New York, 1988; Vol. NATO ASI Series. Ser. A.: Life sciences; pp 179−186.

(18) Ogrodnik, A.; Keupp, W.; Volk, M.; Aumeier, G.; Michel-Beyerle, M. E. *J. Phys. Chem.* **1994**, *98*, 3432−3439.

(19) Kuhn, H. *Phys. Rev. A* **1986**, *34*, 3409−3425.

(20) Zinth, W.; Arlt, T.; Wachtveitl, J. *B. Buns. Phys. Chem.* **1996**, *100*, 1962−1966.

(21) Spörlein, S.; Zinth, W.; Meyer, M.; Scheer, H.; Wachtveitl, J. *Chem. Phys. Lett.* **2000**, *322*, 454−464.

(22) Du, M.; Rosenthal, S. J.; Xie, X.; DiMagno, T. J.; Schmidt, M.; Hanson, D. K.; Schiffer, M.; Norris, J. R.; Fleming, G. R. *Proc. Natl. Acad. Sci. U.S.A.* **1992**, *89*, 8517−8521.

(23) Jia, Y.; DiMagno, T. J.; Chan, C.-K.; Wang, Z.; Du, M.; Hanson, D. K.; Schiffer, M.; Norris, J. R.; Fleming, G. R.; Popov, M. S. *J. Phys. Chem.* **1993**, *97*, 13180−13191.

(24) van Brederode, M. E.; van Mourik, F.; van Stokkum, I. H. M.; Jones, M. R.; van Grondelle, R. *Proc. Natl. Acad. Sci. U.S.A.* **1999**, *96*, 2054−2059.

(25) van Brederode, M. E.; van Stokkum, I. H. M.; Katilius, E.; van Mourik, F.; Jones, M. R.; van Grondelle, R. *Biochemistry* **1999**, *38*, 7545−7555.

(26) Vos, M. H.; Lambry, J.-C.; Robles, S. J.; Youvan, D. C.; Breton, J.; Martin, J.-L. *Proc. Natl. Acad. Sci. U.S.A.* **1991**, *88*, 8885−8889.

(27) Vos, M. H.; Rappaport, F.; Lambry, J. C.; Breton, J.; Martin, J.-L. *Nature* **1993**, *363*, 320−325.

(28) Streltsov, A. M.; Aartsma, T. J.; Hoff, A. J.; Shuvalov, V. A. *Chem. Phys. Lett.* **1996**, *266*, 347−352.

(29) Boxer, S. G.; Stanley, R. J. *J. Phys. Chem.* **1995**, *99*, 859−863.

(30) Spörlein, S.; Zinth, W.; Wachtveitl, J. *J. Phys. Chem. B* **1998**, *102*, 7492−7496.

(31) Fleming, G. R.; Martin, J. L.; Breton, J. *Nature* **1988**, *333*, 190−192.

(32) Breton, J.; Martin, J. L.; Fleming, G. R.; Lambry, J. C. *Biochemistry* **1988**, *27*, 8276−8284.

(33) Lauterwasser, C.; Finkele, U.; Scheer, H.; Zinth, W. *Chem. Phys. Lett.* **1991**, *183*, 471−477.

(34) DeVault, D. *Quantum Mechanical Tunneling in Biological Systems*; University Press: Cambridge, MA, 1984.

(35) Zener, C. *Proc. R. Soc. London* **1932**, *A*, 696−702.

(36) Marcus, R. A.; Sutin, N. *Biochim. Biophys. Acta* **1985**, *811*, 265−322.

(37) Bixon, M.; Jortner, J.; Michel-Beyerle, M. E. *Biochim. Biophys. Acta* **1991**, *1056*, 301−315.

(38) Bixon, M.; Jortner, J. *Chem. Phys. Lett.* **1989**, *159*, 17−20.

(39) Riedle, E.; Beutter, M.; Lochbrunner, S.; Piel, J.; Schenkl, S.; Spörlein, S.; Zinth, W. *Appl. Phys. B* **2000**, *B71*, 457−465.

(40) Lauβermair, E.; Oesterhelt, D. *EMBO J.* **1992**, *11*, 777−783.

(41) Arlt, T.; Bibikova, M.; Penzkofer, H.; Oesterhelt, D.; Zinth, W. *J. Phys. Chem.* **1996**, *100*, 12060−12065.

(42) Arlt, T.; Dohse, B.; Schmidt, S.; Wachtveitl, J.; Laussermair, E.; Zinth, W.; Oesterhelt, D. *Biochemistry* **1996**, *35*, 9235−9244.

(43) Lancaster, C. R. D.; Bibikova, M. V.; Sabatino, P.; Oesterhelt, D.; Michel, H. *J. Biol. Chem.* **2000**, *275*, 39364−39368.

(44) Huppmann, P.; Artl, T.; Penzkofer, H.; Schmidt, S.; Bibikova, M.; Dohse, B.; Oesterhelt, D.; Wachtveitl, J.; Zinth, W. *Biophys. J.* **2002**, *82*, 3186−3197.

(45) Parson, W. W.; Warshel, A. In *The photosynthetic reaction center*.; Deisenhofer, J., Norris, J. R., Eds.; Academic Press: New York, 1993; Vol. II; pp 23−48.

(46) Xu, D.; Schulten, K. *Chem. Phys.* **1994**, *182*, 91−117.

(47) Kolbasov, D.; Scherz, A. *J. Phys. Chem. B* **2000**, *104*, 1802−1809.

(48) McMahon, B. H.; Müller, J. D.; Wraight, C. A.; Nienhaus, G. U. *Biophys. J.* **1998**, *74*, 2567−2587.

(49) Trissl, H. W.; Breton, J.; Deprez, J.; Dobek, A.; Leibl, W. *Biochim. Biophys. Acta* **1990**, *1015*, 322−333.